SUPPLEMENTAL INFORMATION

Annual Partitioning Patterns of Labyrinthulomycetes Reveal Their Multifaceted Role in Marine Microbial Food Webs

Ningdong Xie[1,2], Dana E. Hunt[2,3], Zackary I. Johnson[2,3], Yaodong He[1], Guangyi Wang[1,4#]

[1]Center for Marine Environmental Ecology, School of Environmental Science and Engineering, Tianjin University, Tianjin 300072, China

[2]Marine Laboratory, Duke University, Beaufort NC USA

[3]Biology Department, Duke University, Durham NC USA

[4]Key Laboratory of Systems Bioengineering (Ministry of Education), Tianjin University, Tianjin 300072, China

Running title: Annual community structure of Labyrinthulomycetes in coastal waters

Keywords: Fungus-like protist; coastal ocean; time series; community structure; niche partitioning; microbial interaction

[#]Corresponding author:

Tel: (86) 022-8740210

Fax: (86) 0755-8740210

E-mail: gywang@tju.edu.cn

Figure S1

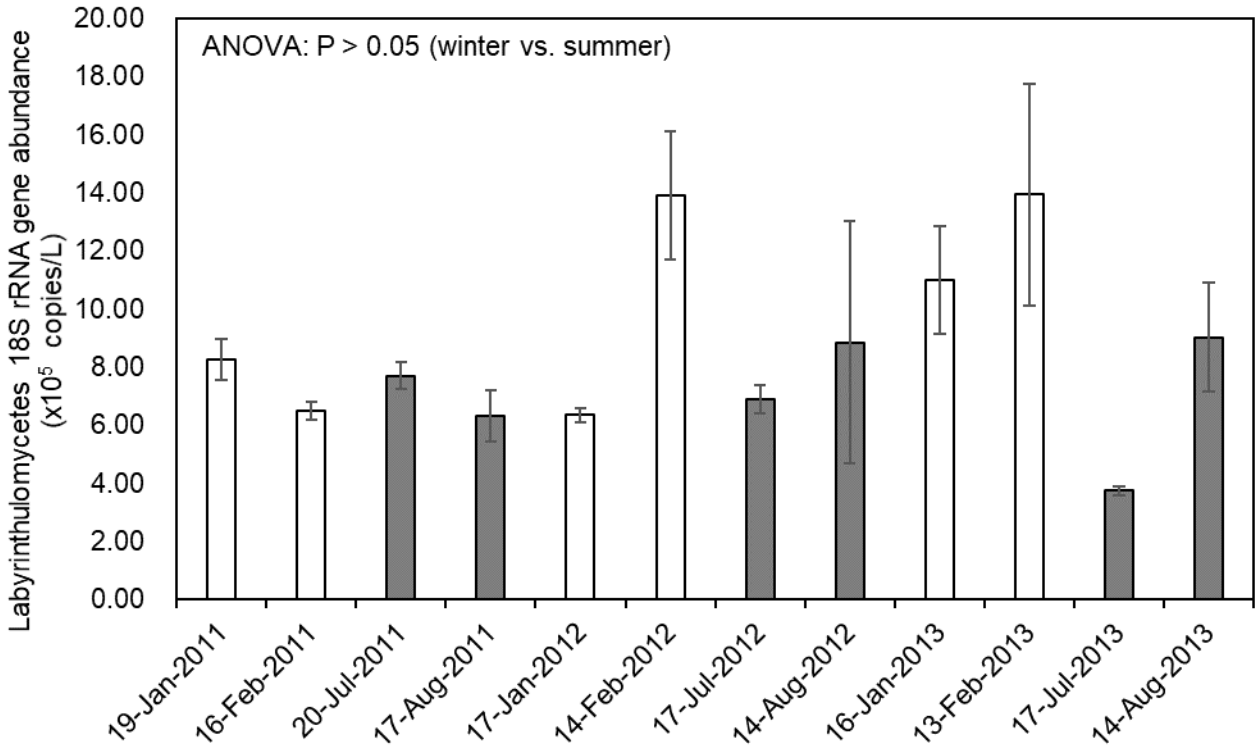

Fig. S1. The Labyrinthulomycetes 18S rRNA gene abundance per liter of seawater for the representative winter (mid-January and mid-February) and summer (mid-July and mid-August) samples across the time series at the Piver's Island Coastal Observatory (PICO) from 2011 to 2013. There was no significant difference between winter and summer samples (ANOVA, $P > 0.05$), shown as grey and white bars, respectively.

Figure S2

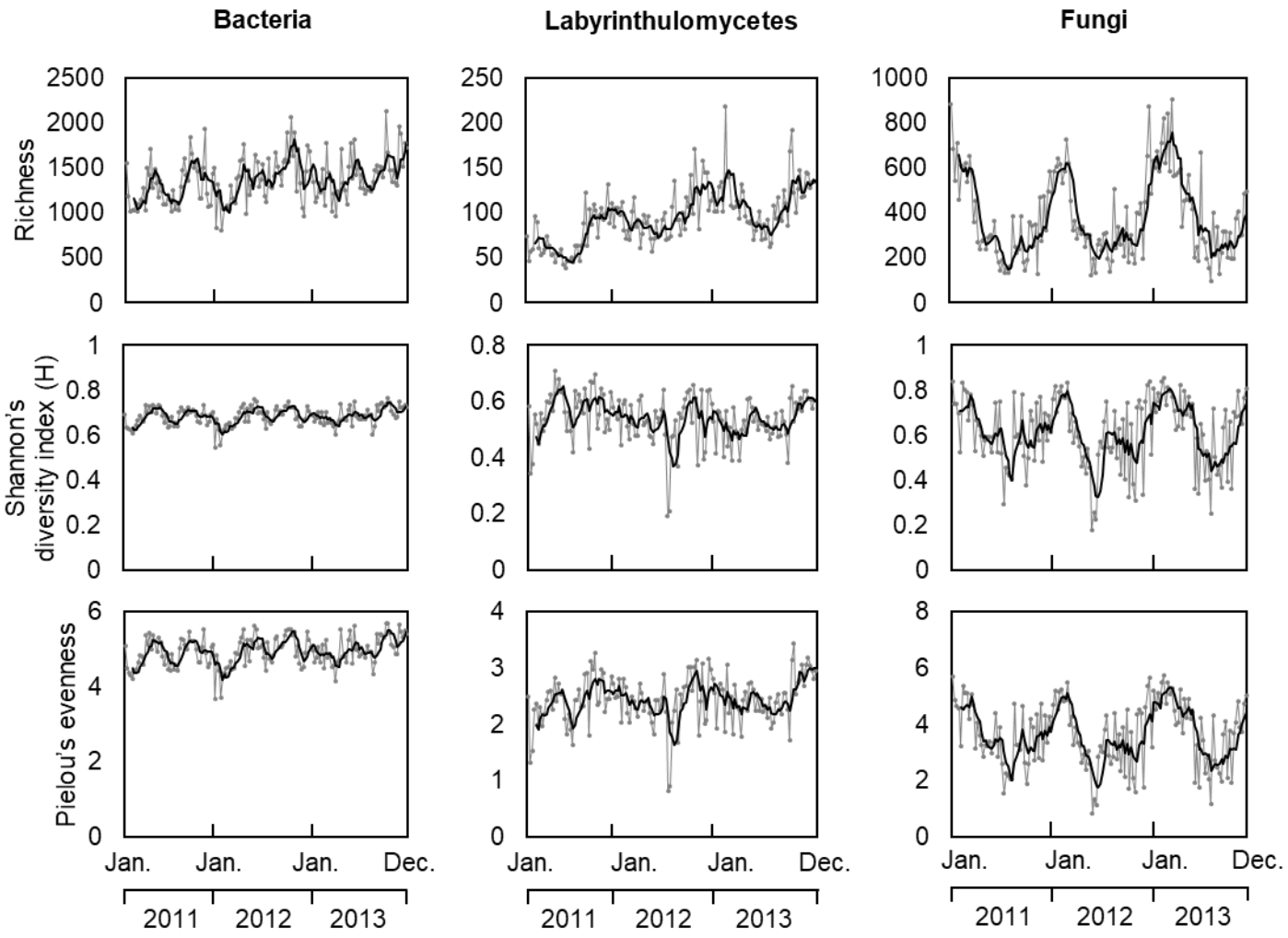

Fig. S2. Comparison for the α-diversity measures between bacteria, fungi, and Labyrinthulomycetes across the weekly time series at Piver's Island Coastal Observatory (PICO) from 2011 to 2013, with the 5-week moving average curves plotted in bold lines.

Figure S3

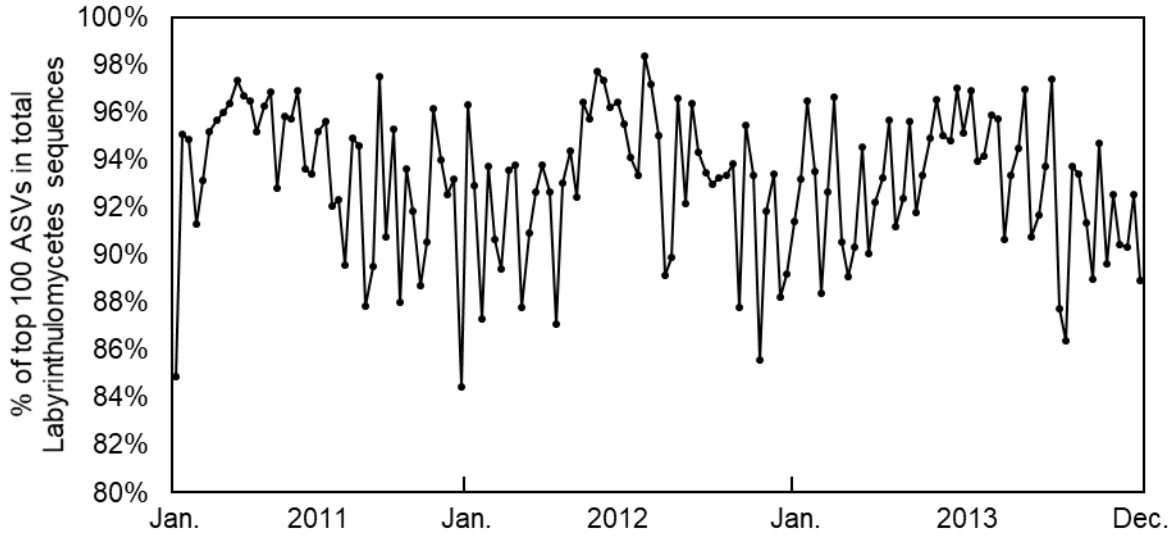

Fig. S3. The relative abundance of the 100 most abundant Labyrinthulomycetes 18S rRNA gene amplicon sequence variants (ASVs) in the total Labyrinthulomycetes ASV sequences across the weekly time series at the Piver's Island Coastal Observatory (PICO) from 2011 to 2013. The average percentage is 93.11%.

Figure S4

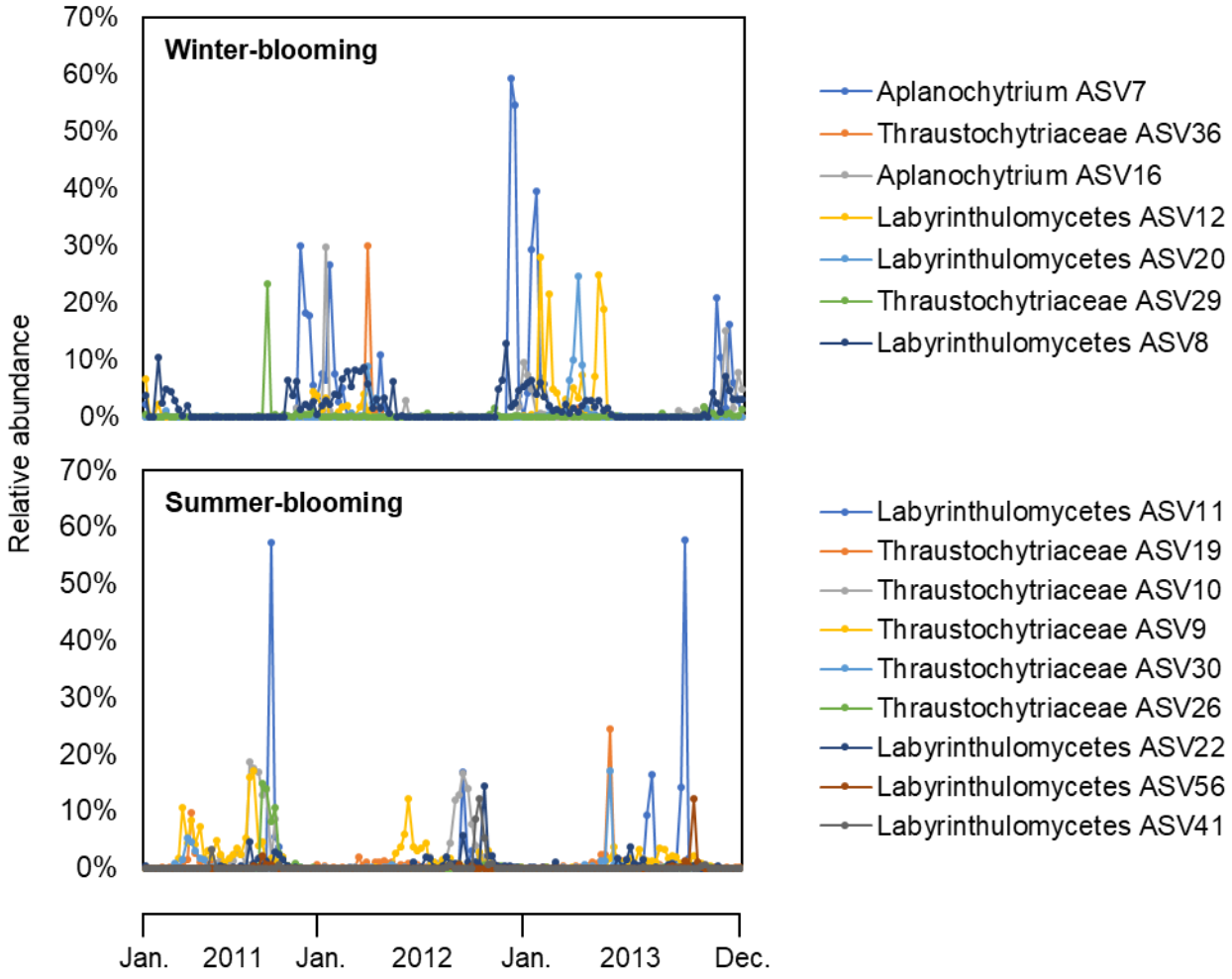

Fig. S4. The abundance dynamics of the winter/summer-blooming (Mfuzz cluster, see Fig. 3) Labyrinthulomycetes 18S rRNA gene amplicon sequence variants (ASVs) across the weekly time series at Piver's Island Coastal Observatory (PICO) from 2011 to 2013. Unlike the persistent ASVs with seasonal preferences (see Fig. S5), the dynamic of the ASVs shown here were dominated by transient blooms. Only ASVs with a maximum relative abundance >10% were plotted as representatives.

Figure S5

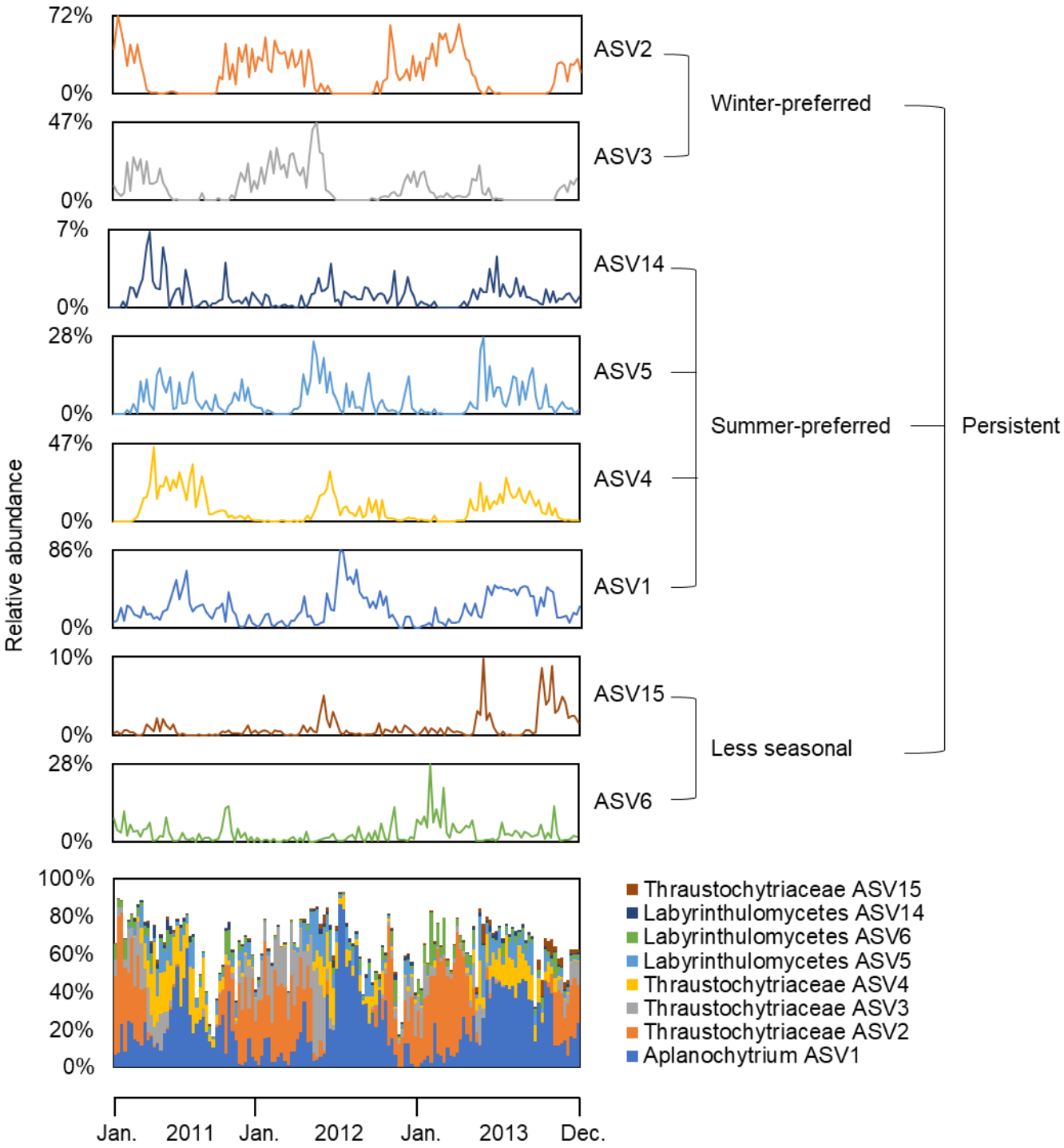

Fig. S5. The abundance dynamics and seasonal preferences of the 8 persistent (Mfuzz cluster, see Fig. 3) Labyrinthulomycetes 18S rRNA gene amplicon sequence variants (ASVs) across the weekly time series at the Piver's Island Coastal Observatory (PICO) from 2011 to 2013.

Figure S6

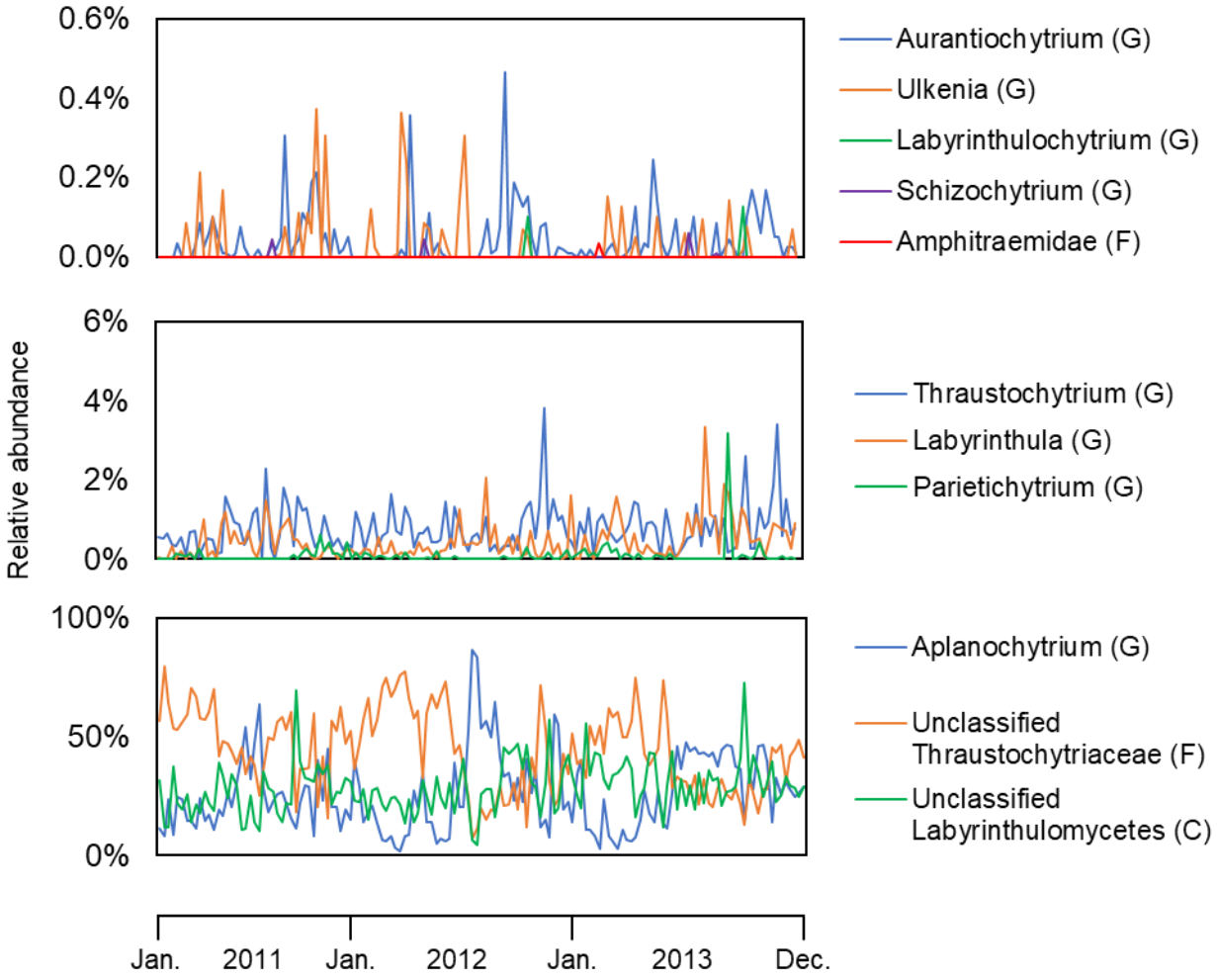

Fig. S6. The relative abundance dynamics of each described genus (G), unclassified family (F), and unclassified class (C) of the Labyrinthulomycetes protists across the weekly time series at the Piver's Island Coastal Observatory (PICO) from 2011 to 2013. The genera *Aurantiochytrium*, *Ulkenia*, *Labyrinthulochytrium*, *Schizochytrium*, *Thraustochytrium*, and *Parietichytrium* belong to the family Thraustochytriaceae, also known as the thraustochytrids sensu stricto.

Figure S7

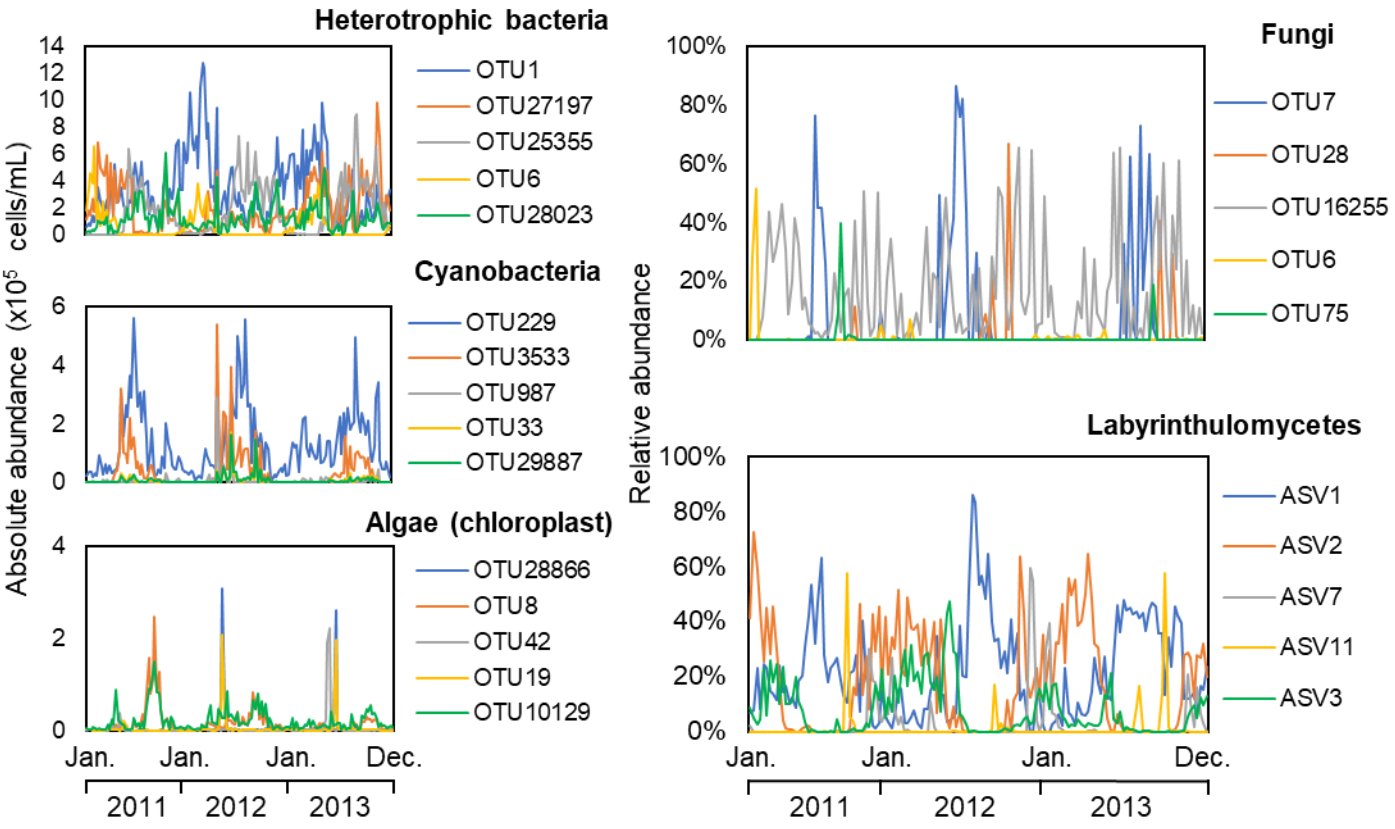

Fig. S7. Comparison for the typical annual patterns of heterotrophic bacteria, cyanobacteria, algae, fungi and Labyrinthulomycetes protists across the weekly time series at the Piver's Island Coastal Observatory (PICO) from 2011 to 2013. Of each group, top 5 phylotypes (OTUs or ASVs) that exhibited the highest maximum abundance across the time series were plotted by their absolute (heterotrophic bacteria, cyanobacteria, and algae) or relative (fungi and Labyrinthulomycetes) abundances.

Figure S8

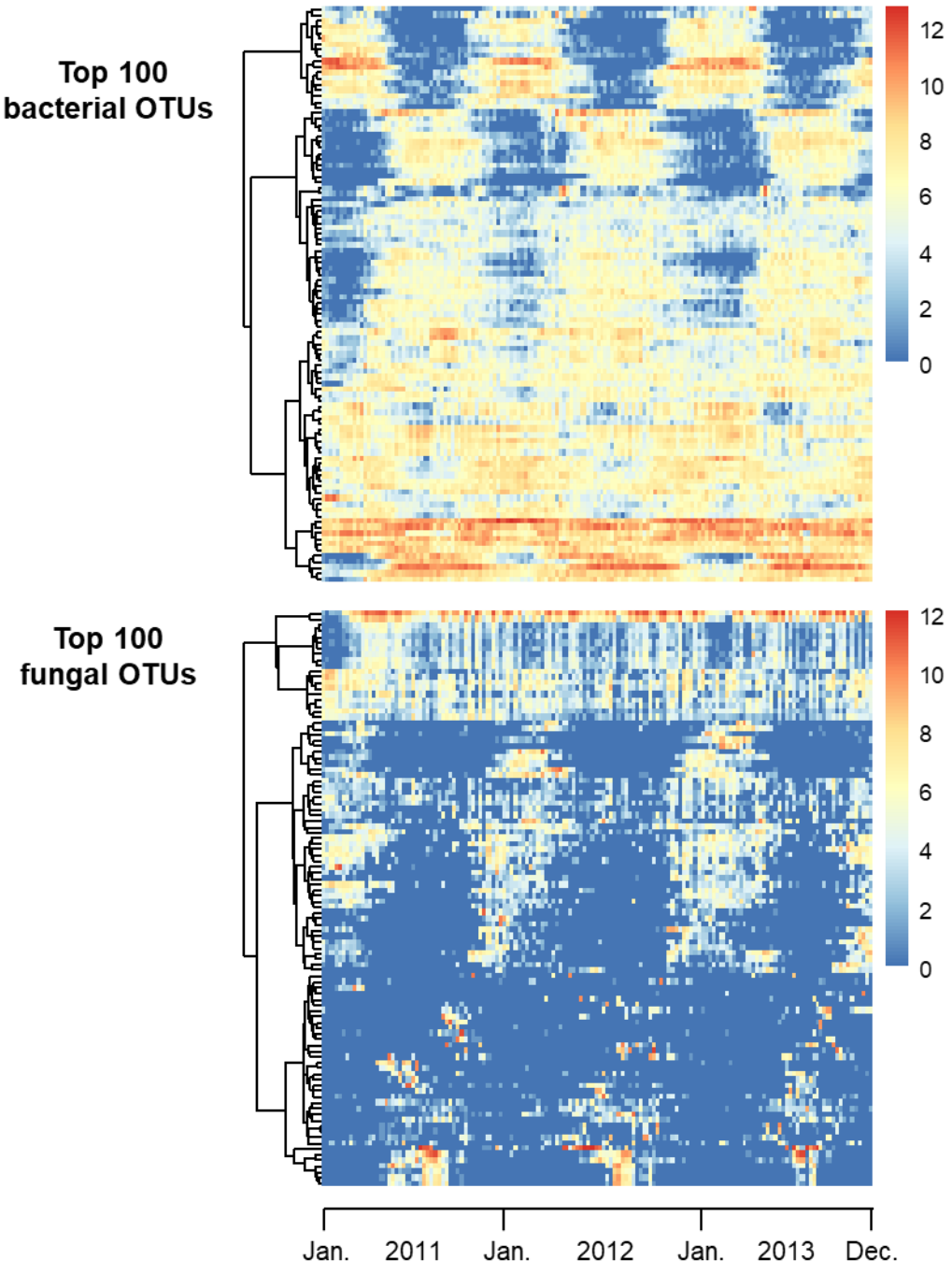

Fig. S8. The heatmaps for the relative abundances of the 100 most abundant bacterial OTUs and 100 most abundant fungal OTUs across the weekly time series at the Piver's Island Coastal Observatory (PICO) from 2011 to 2013. The abundance data were rarified and log-2 transformed. The OTUs were clustered by Ward's minimum variance method.

Table S1

Pearson correlations (R-values) between the environmental parameters and Labyrinthulomycetes 18S rRNA gene amplicon sequence variants (ASV) richness, Shannon's diversity, Pielou's evenness, and total abundance (copies number per liter seawater) at the Piver's Island Coastal Observatory (PICO).

	Richness (N=143)	Shannon's diversity (N=143)	Pielou's evenness (N=143)	Total abundance (N=12)
Fungal abundance	**0.366****	**0.275****	0.120	0.092
Bacterial abundance	**-0.174**	**-0.231***	-0.156	-0.490
Insolation	**-0.536****	**-0.358****	-0.131	-0.446
Temperature	**-0.454****	**-0.222***	-0.018	-0.445
Mean lower low water	0.159	**0.210**	0.164	0.408
Salinity	**-0.433****	-0.094	0.121	-0.346
Oxygen Saturation	**-0.394****	-0.148	0.030	**-0.611**
pH	**-0.483****	-0.082	0.163	-0.515
Dissolved inorganic carbon	**-0.385****	-0.040	0.142	0.062
Chlorophyll *a*	-0.071	-0.057	-0.043	-0.427
NH_4	**0.167**	**0.185**	0.135	0.186
NOx	0.122	**0.177**	0.140	0.083
PO_4	0.010	**0.219***	**0.269***	-0.254
SiO_4	0.067	0.081	0.062	-0.322

Bold numbers indicate the correlations are significant at $P < 0.05$ level;

* Correlations are significant at $P < 0.01$ level;

** Correlations are significant at $P < 0.001$ level.

Table S2

Potential covariations between 100 most abundant Labyrinthulomycetes ASVs and 100 most abundant heterotrophic bacterial OTUs identified by their strong (|R| > 0.6) pairwise Pearson correlations.

Labyrinthulomycetes	Heterotrophic bacteria	R	P[1]
ASV1	OTU50	0.709	5.61E-23
ASV1	OTU8521	0.700	3.03E-22
ASV1	OTU22184	0.660	3.84E-19
ASV1	OTU88	0.649	2.48E-18
ASV1	OTU2	0.646	3.81E-18
ASV1	OTU66	0.636	1.80E-17
ASV1	OTU73	0.626	7.94E-17
ASV1	OTU57	0.614	4.37E-16
ASV1	OTU29893	-0.606	1.31E-15
ASV2	OTU22	0.729	8.67E-25
ASV2	OTU6	0.708	6.51E-23
ASV2	OTU8615	0.676	2.51E-20
ASV2	OTU13	0.641	8.10E-18
ASV2	OTU4011	0.632	3.12E-17
ASV2	OTU32	0.627	7.11E-17
ASV2	OTU40	0.620	1.79E-16
ASV2	OTU18	0.619	2.10E-16
ASV2	OTU22703	0.604	1.74E-15
ASV2	OTU92	-0.603	2.15E-15
ASV2	OTU86	-0.607	1.22E-15
ASV2	OTU88	-0.611	6.49E-16
ASV2	OTU79	-0.613	5.39E-16
ASV2	OTU9	-0.625	9.93E-17
ASV2	OTU50	-0.627	7.23E-17
ASV2	OTU587	-0.637	1.65E-17
ASV2	OTU7	-0.638	1.25E-17
ASV2	OTU191	-0.638	1.44E-17
ASV2	OTU57	-0.713	2.49E-23
ASV3	OTU45	0.638	1.44E-17
ASV3	OTU14	0.626	8.10E-17
ASV3	OTU11968	0.602	2.22E-15
ASV4	OTU86	0.759	7.27E-28
ASV4	OTU9	0.668	1.05E-19
ASV4	OTU191	0.636	1.79E-17
ASV7	OTU143	0.609	8.84E-16
ASV13	OTU8521	0.680	1.42E-20
ASV13	OTU2	0.631	3.82E-17
ASV13	OTU66	0.623	1.27E-16
ASV13	OTU27858	0.612	6.19E-16
ASV13	OTU92	0.601	2.81E-15
ASV24	OTU29715	0.659	5.27E-19
ASV35	OTU2	0.664	2.15E-19
ASV37	OTU22	0.641	9.22E-18
ASV37	OTU81	0.630	4.71E-17
ASV37	OTU1	0.629	5.48E-17
ASV37	OTU6	0.629	5.00E-17
ASV37	OTU32	0.615	4.11E-16
ASV54	OTU32	0.626	8.21E-17
ASV55	OTU35	0.655	9.50E-19
ASV58	OTU98	0.639	1.14E-17

[1] P value not corrected for multiple hypothesis testing

Table S3

Potential covariations between 100 most abundant Labyrinthulomycetes ASVs and 100 most abundant phytoplankton (including cyanobacteria and chloroplasts) OTUs identified by their strong (|R| > 0.6) pairwise Pearson correlations.

Labyrinthulomycetes	Phytoplankton	R	P[1]
ASV1	OTU41	0.627	6.84E-17
ASV2	OTU27293	-0.602	2.20E-15
ASV4	OTU3533	0.630	4.67E-17
ASV4	OTU28330	0.794	5.17E-32
ASV4	OTU228	0.741	6.08E-26
ASV6	OTU11985	0.612	5.53E-16
ASV10	OTU10129	0.641	8.45E-18
ASV10	OTU8	0.651	1.73E-18
ASV10	OTU4017	0.653	1.30E-18
ASV10	OTU17944	0.636	1.70E-17
ASV10	OTU10151	0.635	2.24E-17
ASV10	OTU119	0.612	5.61E-16
ASV12	OTU42	0.601	2.72E-15
ASV26	OTU10129	0.632	3.33E-17
ASV26	OTU8	0.746	1.81E-26
ASV26	OTU4017	0.608	1.02E-15
ASV26	OTU26074	0.849	1.53E-40
ASV26	OTU17944	0.651	1.70E-18
ASV26	OTU10151	0.717	1.18E-23
ASV26	OTU27801	0.607	1.23E-15
ASV26	OTU18292	0.672	5.47E-20
ASV26	OTU2696	0.638	1.45E-17
ASV29	OTU26074	0.643	6.19E-18
ASV33	OTU101	0.724	2.30E-24
ASV54	OTU38	0.653	1.33E-18
ASV54	OTU25541	0.927	1.66E-61
ASV56	OTU389	0.682	9.99E-21
ASV56	OTU23216	0.600	3.04E-15
ASV63	OTU6962	0.608	1.07E-15
ASV71	OTU34	0.606	1.39E-15
ASV71	OTU22245	0.626	7.89E-17
ASV71	OTU389	0.619	2.13E-16
ASV71	OTU23216	0.656	7.52E-19
ASV94	OTU8974	0.605	1.57E-15
ASV95	OTU987	0.722	3.94E-24
ASV98	OTU10151	0.600	2.90E-15

[1] P value not corrected for multiple hypothesis testing

Table S4

Potential covariations between 100 most abundant Labyrinthulomycetes ASVs and 100 most abundant fungal OTUs identified by their strong (|R| > 0.6) pairwise Pearson correlations.

Labyrinthulomycetes	Fungi	R	P[1]
ASV6	OTU33	0.688	1.60E-20
ASV11	OTU78	0.698	2.78E-21
ASV11	OTU99	0.664	9.24E-19
ASV20	OTU59	0.878	4.28E-45
ASV20	OTU24	0.743	2.86E-25
ASV22	OTU66	0.808	9.30E-33
ASV29	OTU72	0.731	3.33E-24
ASV38	OTU12980	0.714	1.13E-22
ASV51	OTU51	0.617	9.47E-16
ASV54	OTU23	0.610	2.65E-15
ASV55	OTU177	0.625	3.09E-16
ASV59	OTU66	0.849	3.18E-39
ASV61	OTU28	0.649	9.31E-18
ASV64	OTU41	0.780	3.04E-29
ASV68	OTU168	0.706	5.71E-22
ASV76	OTU96	0.623	4.20E-16
ASV81	OTU10058	0.674	1.74E-19
ASV89	OTU206	0.832	2.11E-36

[1] P value not corrected for multiple hypothesis testing

Table S5

Evaluation of Maximum Likelihood fits of 24 different nucleotide substitution models, using aligned representative and reference sequences that were prepared for the Labyrinthulomycetes phylogenetic analyses.

Model	Parameters	BIC	AICc	lnL	(+I)	(+G)	R
GTR+G+I	257	11815.68	9578.302	-4530.67	0.38	0.32	1.23
T92+G+I	251	11819.46	9634.254	-4564.72	0.38	0.33	1.29
HKY+G+I	253	11832.37	9629.774	-4560.46	0.38	0.33	1.3
K2+G+I	250	11837.22	9660.707	-4578.96	0.38	0.32	1.28
TN93+G+I	254	11843.49	9632.201	-4560.66	0.37	0.33	1.28
T92+G	250	11850.22	9673.71	-4585.46	n/a	0.21	1.28
TN93+G	253	11855.93	9653.334	-4572.24	n/a	0.2	1.27
GTR+G	256	11859.29	9630.614	-4557.84	n/a	0.21	1.12
HKY+G	252	11861.4	9667.497	-4580.33	n/a	0.21	1.29
K2+G	249	11867.56	9699.743	-4599.48	n/a	0.21	1.26
JC+G+I	249	11959.85	9792.032	-4645.63	0.36	0.31	0.5
JC+G	248	11990.31	9831.183	-4666.22	n/a	0.21	0.5
T92+I	250	12641.82	10465.3	-4981.25	0.57	n/a	1.13
GTR+I	256	12644.34	10415.66	-4950.36	0.57	n/a	1.14
HKY+I	252	12648.22	10454.32	-4973.74	0.57	n/a	1.15
TN93+I	253	12654.74	10452.15	-4971.64	0.57	n/a	1.14
K2+I	249	12657.05	10489.24	-4994.23	0.57	n/a	1.13
JC+I	248	12773.36	10614.24	-5057.74	0.57	n/a	0.5
GTR	255	13741.19	11521.2	-5504.15	n/a	n/a	1.09
TN93	252	13749.4	11555.5	-5524.33	n/a	n/a	1.09
T92	249	13759.73	11591.91	-5545.57	n/a	n/a	1.08
HKY	251	13764.01	11578.81	-5536.99	n/a	n/a	1.08
K2	248	13774.63	11615.5	-5558.38	n/a	n/a	1.08
JC	247	13885.49	11735.06	-5619.17	n/a	n/a	0.5

Models with the lowest BIC scores (Bayesian Information Criterion) are considered to describe the substitution pattern the best. For each model, AICc value (Akaike Information Criterion, corrected), Maximum Likelihood value (lnL), and the number of parameters (including branch lengths) are also presented. Non-uniformity of evolutionary rates among sites may be modeled by using a discrete Gamma distribution (+G) with 5 rate categories and by assuming that a certain fraction of sites are evolutionarily invariable (+I). Whenever applicable, estimates of gamma shape parameter and/or the estimated fraction of invariant sites are shown. Assumed or estimated values of transition/transversion bias (R) are shown for each model, as well. For estimating ML values, a tree topology was automatically computed. The analysis involved 125 nucleotide sequences. All positions with less than 95% site coverage were eliminated. There were a total of 362 positions in the final dataset. Evolutionary analyses were conducted in MEGA7. Abbreviations: GTR: General Time Reversible; HKY: Hasegawa-Kishino-Yano; TN93: Tamura-Nei; T92: Tamura 3-parameter; K2: Kimura 2-parameter; JC: Jukes-Cantor.